A Compact V-Band Bandpass Filter in IPD Technology

Chih-Yin Hsiao, Shawn S. H. Hsu, and Da-Chiang Chang

***Abstract*—This work presents a miniaturized bandpass filter in V-band using integrated passive device (IPD) technology with thick metal layers and Benzocyclobutene (BCB) dielectric on a glass substrate. The proposed filter, comprised of two stepped-impedance resonators with quarter-wave short-circuited stubs and floating pads, has low passband insertion loss and high stopband attenuation in a compact size. The fabricated filter has an insertion loss of 2.46 dB at the center frequency of 59 GHz, and a 3 dB bandwidth from 55.7 to 62.2 GHz. The core size of this filter is only 0.32×0.4 mm^2 $(0.064 \times 0.08\lambda_0^2)$.**

***Index Terms*—Filter, integrated passive device (IPD), resonator, V-band.**

I. Introduction

INTEGRATION of passive components with active circuits is of critical importance for realizing low cost and compact wireless communication systems. Fabricated on a different substrate, integrated passive device (IPD) process [1], [2] allows stacking the area-consuming passive elements on the active circuits to reduce the size of a system. The IPD technology also improves the performance of passive devices using more flexible materials and processes compared to the standard IC technology.

In this study, a V-band bandpass filter is realized in IPD technology. Recently, the applications of V-band wireless communications such as wireless HD and V-band WLAN attract much attention [3]. The front-end filter plays a critical role in such V-band systems, and many studies in different technologies have been reported on this topic [4]–[9]. In this letter, we design a bandpass filter using cascaded open-loop resonators by stepped-impedance lines in a folded topology. The short-circuited stubs are employed to enhance the stopband attenuation, and the floating pads are used to provide more design freedom to achieve the desired passband characteristic. Measured results demonstrate an insertion loss of 2.46 dB at 59 GHz within a core area of only 0.128 mm ^{2}.

Manuscript received May 17, 2011; accepted August 09, 2011. Date of publication September 01, 2011; date of current version October 07, 2011. This work was supported in part by the National Science Council under Contract NSC 97-2221-E-007-107-MY3.

Chih-Yin Hsiao and S. S. H. Hsu are with the Department of Electrical Engineering and Institute of Electronics Engineering, National Tsing Hua University, Hsinchu 30013, Taiwan (e-mail: shhsu@ee.nthu.edu.tw).

D.-C. Chang is with the National Chip Implementation Center (CIC), Hsinchu 300, Taiwan.

Color versions of one or more of the figures in this letter are available online at http://ieeexplore.ieee.org.

Digital Object Identifier 10.1109/LMWC.2011.2165534

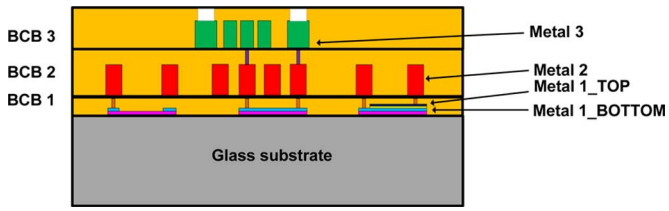

Fig. 1. Cross section of the integrated passive device (IPD) technology used in this study.

II. Integrated Passive Device Technology

In modern silicon IC technology, the quality factor of passive components is mainly limited by the substrate loss and the resistive loss of the metal lines. The IPD technology adopted here uses a high resistivity ($\sim 10^{14}\Omega\cdot\mathrm{m}$) glass substrate, a low loss tangent ($\sim 8\times10^{-4}$) dielectric material benzocyclobutene (BCB), and high conductivity (5.8×10^7 S/m) copper layers to realize passive components with excellent performance. Fig. 1 illustrates the cross section of the IPD process, which is formed by three BCB layers with the thicknesses of 3.7 (BCB 1), 12 (BCB 2), and 10 (BCB 3), respectively, on the glass substrate. The layers Metal 3 and Metal 2 are made of copper with thicknesses of 6 and 10 μm, respectively, and the minimum spacing and minimum line width are both 10 μm. A thin layer (0.25 μm) of Ta $_2$ O $_5$ between Metal 1_TOP and Metal 1_BOTTOM is available for realizing high density capacitors. These two metal layers are made of aluminum with a thickness of 1 μm. With the thick metal layers, low loss tangent dielectric, and high resistivity substrate, the IPD technology is suitable for the applications of V-band filters.

III. Filter Design

The basic structure (simplified) of the proposed bandpass filter is shown in Fig. 2(a), where $l_1 = 90$ μm, $l_2 = 270$ μm, $g_1 = 40$ μm, and $g_2 = 10$ μm. The guiding structure of this design is the coupled half-wavelength open-loop resonators [10], [11]. A pair of folded open-loop resonator is coupled through the fringing fields with a mixed coupling mechanism. In this design, both resonators are synchronously tuned to have a bandstop characteristic with a resonant frequency at around f_0 of the filter. By properly designed coupling between the two resonators, a well-defined bandpass characteristic can be achieved. Differing from the previous studies, the open-ends of the resonators are aligned in the same direction resulting in mixed-mode (both electric and magnetic) coupling of the resonators to enhance the coupling efficiency and reduce insertion loss. Also, taking the advantage of the low loss glass substrate,

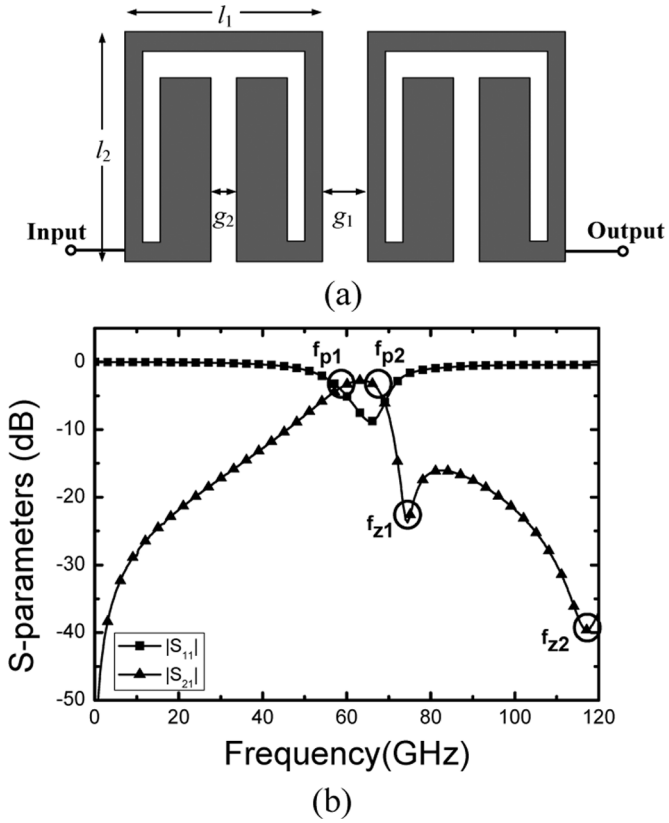

Fig. 2. Bandpass filter with two cascaded resonators: (a) layout view (b) EM simulated S_{21} and S_{11} of the filter.

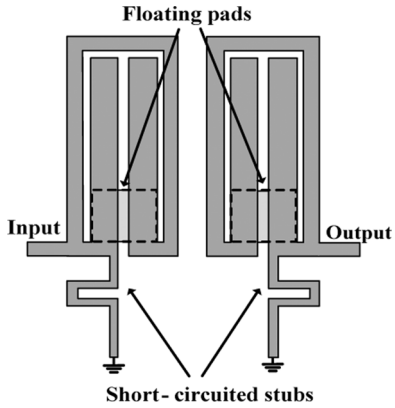

Fig. 3. Layout of the proposed bandpass filter constructed by cascaded resonators with short-circuited stubs and floating pads.

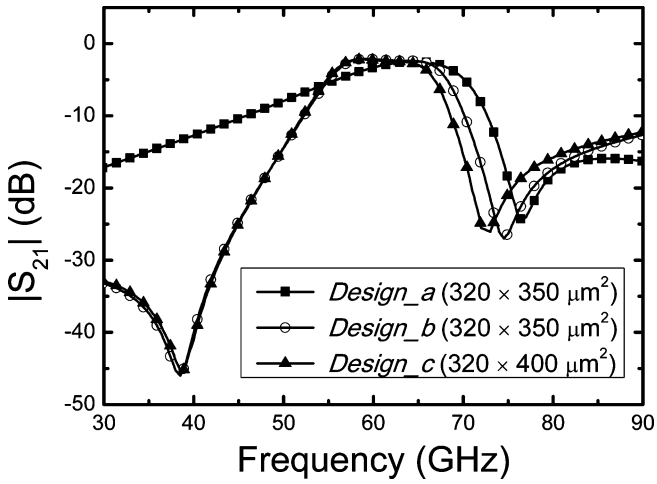

Fig. 4. EM simulated results of three filters with a similar basic structure.

the structure is realized without the ground plane underneath the resonators. Instead, the floating pads are employed to optimize the overall filter characteristic as will be explained later.

Fig. 2(b) is the EM simulation result of the filter, which presents a second-order bandpass characteristic with two transmission poles $f_{\rm p1}$ and $f_{\rm p2}$, and two transmission zeros $f_{\rm z1}$ and $f_{\rm z2}$. The low frequency pole $f_{\rm p1}$ strongly depends on the capacitance originating from the electric coupling between the two resonators, which is mainly determined by g_1. The high frequency pole $f_{\rm p2}$ can be adjusted by the gap g_2 between the two folded low-impedance lines of the single resonator. For the high-frequency stopband attenuation of the filter, the transmission zeros $f_{\rm z1}$ and $f_{\rm z2}$ play important roles. They are closely related to the transmission zero $f_{\rm z}$ of the single resonator, and also the magnetic coupling between the two resonators. These points can be verified by EM simulation.

One major concern of the filter characteristic, as shown in Fig. 2, is the rather slow stopband attenuation in the low frequency range. In the final design, two short-circuited stubs are added to increase the attenuation. As shown in Fig. 3 of the final layout, the quarter-wave stubs are connected to the ground creating an additional transmission zero to enhance the stopband attenuation. As the length of the stubs increases, the frequency of the zero moves toward lower frequencies. This zero is located at around 40 GHz with a stub length of 200 μm.

As mentioned earlier, the conventional microstrip structure is not adopted for the resonators. With the relatively small distance between the metal layers, adding the ground plane to the resonator introduce a large capacitance, which makes $f_{\rm z1}$ too close to $f_{\rm p2}$, leading to an increased insertion loss in passband. Without the ground plane, the floating pads underneath the resonators are used to provide desired capacitance for $f_{\rm p2}$ and $f_{\rm z1}$ optimization. The Metal 1_TOP layer is used for the floating pad with a size of 70 μm $\times$ 50 μm each. Also, the floating pads increase the capacitance and slightly reduce the size of the resonators. In the final layout, l_1 remains unchanged and l_2 reduces to 250 μm, and the core size is only 320 μm $\times$ 400 μm including the input/output feeding lines (50 μm of each port).

Fig. 4 shows the EM simulated results of three different designs denoted as (a), (b), and (c), which have a similar basic structure of cascaded open-loop resonators. Compared with the structure in Fig. 2(a) (*Design_a*), the low frequency stopband attenuation is greatly improved by adding the short-circuited stubs due to the introduced transmission zero (*Design_b*). With the additional floating pads (*Design_c*), $f_{\rm p2}$ and $f_{\rm z1}$ can be adjusted, leading to a better confined bandwidth, and increased capacitance resulting in a smaller filter size.

IV. Measurement Results and Discussion

Fig. 5 shows the micrograph of the filter fabricated in IPD technology. The filter is mainly realized by the Metal 3 layer with a size of 0.426 mm ^{2} (core size: 0.128 mm ^{2}) including the

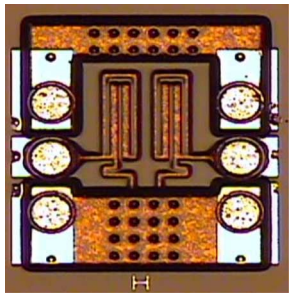

Fig. 5. Micrograph of the proposed V-band bandpass filter in IPD.

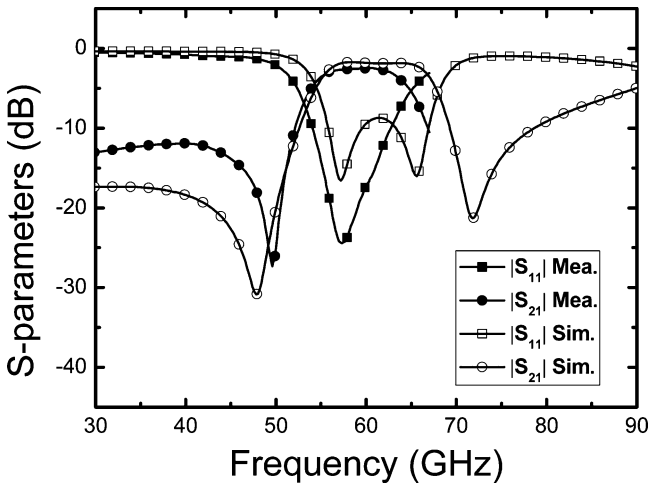

Fig. 6. Comparison of the measured and simulated S_{21} and S_{11} of the IPD bandpass filter.

RF probing pads. The S-parameters were measured on-wafer from 10 MHz to 67 GHz. Fig. 6 presents the measured and simulated S_{21} and S_{11} of the filter. The measured f_0 is $\sim$59 GHz and the insertion loss is only 2.46 dB at f_0 associated with a return loss of greater than 24 dB. The simulation is performed by SONNET (using a grid size of 1 μm) including the pads and surrounding metal plane, which could be considered as part of the filter in actual applications for flip-chip integration. Based on the measured S-parameters, the normalized attenuation and phase constant of the filter can be calculated [12], ranging from 0.28 to 0.45 and 1.1 to 2.6, respectively, within the 3 dB bandwidth. The loaded quality factor is 5.2 and the unloaded quality factor is 20.3. Table I summaries the filter performance and compares with prior arts of V-band filters realized in both standard CMOS [7], [8] and other technologies using low-loss substrates similar to IPD [4]–[6], or MEMS technology [9]. It should be pointed out that a lower insertion loss achieved in [8] can be mainly attributed to the smaller feature size in advanced CMOS technology. The smaller spacing allows a tight coupling and hence a reduced insertion loss.

V. Conclusion

This work presented a miniaturized open-loop resonator filter in V-band using the IPD process with a low loss glass substrate and thick metal layers. The proposed filter topology, consisting of two cascaded resonators with mixed coupling design, demonstrated an insertion loss of only 2.46 dB at 59 GHz within a core area of only 0.128 mm ^{2}.

TABLE I
Performance Comparison With Prior Arts

	f_0 (GHz)	S_{21} (dB)	BW	Size ($mm^2/\lambda_0^2\times10^{-2}$)	Process
This work	59	2.46	11%	0.426/1.704 0.128/0.512 (core)	IPD
[4]	62	3	3.3%	18/76.88	IWG(1)
[5]	59.1	5	6.9%	4.59/17.8 1.12/4.347 (core)	LTCC(2)
[6]	63.5	2.97	2.4%	4.2/19	LTCC
[7]	70	3.6	25%	0.435/2.37 (core)	0.18μm CMOS
[8]	61.5	1.5	14.6%	0.21/0.8755 (core)	0.13μm CMOS
[9]	65	3.3	10%	1.27/5.974	MEMS

(1) Integrated waveguide.
(2) Low-temperature co-fired ceramics.

References

[1] H.-K. Chen, Y.-C. Hsu, T.-Y. Lin, D.-C. Chang, Y.-Z. Juang, and S.-S. Lu, "CMOS wideband LNA design using integrated passive device," in *IEEE MTT-S Int. Dig.*, Jun. 2009, pp. 673–676.

[2] H. Lee, C. Park, and S. Hong, "A quasi-four-pair class-E CMOS RF power amplifier with an integrated passive device transformer," *IEEE Trans. Microw. Theory Tech.*, vol. 57, no. 4, pp. 752–759, Apr. 2009.

[3] S. E. Gunnarsson, C. Karnfelt, H. Zirath, R. Kozhuharov, D. Kuylenstierna, C. Fager, M. Ferndahl, B. Hansson, A. Alping, and P. Hallbjorner, "60 GHz single-chip front-end MMICs and systems for multi-Gb/s wireless communication," *IEEE J. Solid-State Circuits*, vol. 42, no. 5, pp. 1143–1157, May 2007.

[4] S. T. Choi, K. S. Yang, K. Tokuda, and Y. H. Kim, "A V-band planar narrow bandpass filter using a new type integrated waveguide transition," *IEEE Microw. Wireless Compon. Lett.*, vol. 14, no. 12, pp. 545–547, Dec. 2004.

[5] K. Nishikawa, S. Tomohiro, T. Ichihiko, and K. Shuji, "Compact 60-GHz LTCC stripline parallel-coupled bandpass filter with parasitic elements for millimeter-wave system-on-package," in *IEEE MTT-S Int. Dig.*, Jun. 2007, pp. 1649–1652.

[6] J.-H. Lee, S. Pinel, J. Laskar, and M. M. Tentzeris, "Design and development of advanced cavity-based dual-mode filters using low-temperature co-fired ceramic technology for V-band gigabit wireless systems," *IEEE Trans. Microw. Theory Tech.*, vol. 55, no. 9, pp. 1869–1879, Sep. 2007.

[7] C.-Y. Hsu, C.-Y. Chen, and H.-R. Chuang, "70 GHz folded loop dual-mode bandpass filter fabricated using 0.18 μm standard CMOS technology," *IEEE Microw. Wireless Compon. Lett.*, vol. 18, no. 9, pp. 587–589, Sep. 2008.

[8] B. Yang, E. Skafidas, and R. J. Evans, "Design of 60 GHz millimetre-wave bandpass filter on bulk CMOS," *IET Trans. Microw., Antennas Propag*, vol. 3, no. 6, pp. 943–949, Sep. 2009.

[9] H.-T. Kim, J.-H. Park, Y.-K. Lim, and Y. Kwon, "Low-loss and compact V-band MEMS-based analog tunable bandpass filters," *IEEE Microw. Wireless Compon. Lett.*, vol. 12, no. 11, pp. 432–434, Nov. 2002.

[10] J. S. Hong and M. J. Lancaster, "Canonical microstrip filter using square open-loop resonators," *IEE Electron. Lett.*, vol. 31, no. 23, pp. 2020–2022, Nov. 1995.

[11] J. S. Hong, "Couplings of asynchronously tuned coupled microwave resonators," *Proc. Inst. Elect. Eng.*, vol. 147, no. 5, pp. 354–358, Oct. 2000.

[12] H.-K. Wu, H.-S. Wu, and C.-K. C. Tzuang, "Electric-magnetic-electric slow-wave microstrip line and bandpass filter of compressed size," *IEEE Trans. Microw. Theory Tech.*, vol. 50, no. 8, pp. 1996–2004, Aug. 2002.